https://doi.org/10.1016/j.nucengdes.2019.110392

NACIE-UP POST-TEST SIMULATIONS BY CFD CODES

A. Pucciarelli[a*], G. Barone[a], N. Forgione[a], F. Galleni[a], D. Martelli[b]

[a] Dipartimento di Ingegneria Civile e Industriale, Università di Pisa, L.go Lucio Lazzarino n. 2, Pisa, Italy

[b] Experimental Engineering Division, Fusion and Technology for Nuclear Safety and Security Department ENEA Brasimone Research Centre, 40032 Camugnano (BO), Italy

[*]Corresponding author E-mail: andrea.pucciarelli@dici.unipi.it

ABSTRACT

The paper concerns about CFD calculations of LBE flowing in the wire-wrapped hexagonal array electrical pin bundle of NACIE-UP facility. Pressure drop and friction factor analyses are performed in order to find possible matching between CFD results and available correlations to be used in the frame of forthcoming applications involving CFD/System Codes (STH) coupling calculations. The Fuel Pin Simulator of the NACIE-UP facility is presently considered for calculations; post-test analyses are performed as well in order to understand capabilities and uncertainties of available CFD codes and techniques in the liquid metal thermal hydraulics field. Calculations were performed using the commercial codes STAR-CCM+ and ANSYS FLUENT and promising results were provided. In particular, good matching between CFD results and predictions from the Cheng and Todreas (1986) correlation is observed in the frame of the pressure drop analysis. Post-test analyses aiming at comparing the measured and calculated temperature values for three selected operating conditions were performed; the adopted CFD tool reported good capabilities in reproducing the experimental results. Sensitivity analyses considering anomalous power distributions were also performed. The lesson drawn provided further comprehension of the involved phenomena and interesting information for future applications involving CFD/STH codes in coupling calculations.

https://doi.org/10.1016/j.nucengdes.2019.110392

INTRODUCTION

Since the early 2000s, Liquid Metal Fast Reactors (LMFRs) have been considered among the possible systems to be selected for the upcoming new Generation IV of nuclear power plants (GIF, 2014). Among the various goals of the present development, sustainability, safety and reliability definitively represent the key issues; in this sense Lead Bismuth Eutectic (LBE) represents a valuable candidate for reactor cooling for both its nuclear and thermal-hydraulic properties and capabilities. In particular, being a dense fluid, it shows optimal cooling capabilities and its high boiling point significantly precludes the possibility of coolant boiling, paving the way for a safe use in both forced and natural circulation conditions. On the other hand, the available literature on liquid metal thermal hydraulics behaviour is not as wide as for water, mostly due to the limited availability of experimental data and the actual difficulties in collecting information and measurements adopting the standard detection devices. Consequently, in the liquid metal field, building up new facilities and running new experiments play a key role in helping to broaden and improving the present comprehension and understanding of the involved phenomena.

In this sense, the experimental campaigns carried out at ENEA-Brasimone R.C during the past decade (NACIE-UP, Di Piazza et al., 2013; CIRCE-ICE, Tarantino et al., 2011; CIRCE-HERO, Pesetti et al., 2018) represent a valuable workbench for testing LBE thermal hydraulics in different flow regimes. In this context, the University of Pisa performed several numerical analyses, both by CFD and STH codes, of the addressed experimental conditions providing support and a deeper insight in the involved phenomena (Martelli et al., 2014, Narcisi et al, 2017, Martelli et al., 2017a, Gonfiotti et al., 2018). The present work focuses on CFD analyses aiming at reproducing some of the results collected in the frame of the experimental campaign involving the NACIE-UP facility. It mainly consists of two phases, pressure drop and friction factor analyses and post-test analyses; the final goal is paving the way for the coupled CFD-STH Codes application.

Setting up suitable correlations for STH codes and validating CFD codes for pressure drop analysis is of capital importance for the development of LMFRs, because of their reliance on natural circulation for abnormal and accidental conditions. In literature, several correlations exist for the prediction of pressure drops in wire-wrapped hexagonal array pin bundles, to which the Fuel Pin Simulator (FPS) allocated in the NACIE-UP facility may be compared. In particular, the Cheng and Todreas (1986) correlation showed interesting capabilities in the frame of other experiences, involving e.g. the RELAP5/MOD3.3 system code (Forgione et al., 2018), and promising matching were observed also in CFD applications (adopting e.g. ANSYS-CFX as in Marinari, 2014). This correlation is consequently considered as a reference in the present work: isothermal calculations varying the imposed mass flow rate and temperature, thus investigating a sufficiently wide Reynolds number range, were performed in the present work, a good matching between the CFD prediction and the considered correlation was obtained.

Post-test analyses involving the comparison of measured and calculated temperature trends were performed as well. Different parameters and flow conditions, taking into account possible uncertainty ranges in the

https://doi.org/10.1016/j.nucengdes.2019.110392

imposed operating conditions, were considered in order to improve the matching between the calculated and measured data. In particular, a sensitivity analysis on the effect of variations of turbulent Prandtl number was performed.

The obtained results provided interesting information and suggest promising developments for future applications involving both STH codes and STH/CFD Codes coupled applications (see e.g. Martelli et al., 2017b). In fact, by recognising the Cheng and Todreas correlation as a valuable tool to be adopted in STH codes providing coherent results between STH and CFD codes for pressure drops across wire-wrapped fuel bundles, it may help in making it simpler setting up coupled calculations and improving the coupled applications predicting capabilities.

NACIE-UP FACILITY DESCRIPTION AND CFD DISCRETIZATION

Test-section description

The NACIE-UP facility (Di Piazza et al., 2013) consists in a rectangular shaped loop created for the investigation of forced and mixed circulation phenomena occurring when using Lead Bismuth Eutectic (LBE); its scheme is reported in Figure 1a. The vertical sides (5.578 m high) represent the riser and downcomer while the horizontal sides, 2.4 m long, simply connect the relevant regions and provide the loop closure. The Fuel Pin Simulator (FPS) is allocated at the bottom of the riser, the Heat Exchanger (HX) is instead positioned at the top of the downcomer: the distance in height between the centre of the heated region of the FPS and the centre of the HX is 4.8 m, which is sufficiently high for the establishment of natural circulation conditions. The Heat Exchanger is divided into two parts, the former, at the top, used for low power applications, the latter, at the bottom, used instead for high power applications; here LBE transfers heat to water, which flows inside the secondary loop. Circulation may also be promoted by the presence of an Argon injection device positioned downstream the FPS; varying the Argon mass flow rate allows simulating different operating and possible incidental conditions. Argon is eventually collected in an expansion vessel positioned at the top of the riser: here Argon is mostly separated from LBE thus relevantly limiting its presence in the downcomer. The expansion vessel also works as a pressurizer accommodating the thermal expansion of LBE, Argon is also used as cover gas in order to prevent the occurrence of oxidation.

The FPS consists in a 1.33 m long hexagonal duct housing an electrically heated 19 rod bundle simulating the fuel pin ranks and it is subdivided into three parts: an entrance unheated region 615 mm long, an active region of 600 mm and a final unheated discharge region of 115 mm. Figure 1b reports the sketch of the cross section taken in the centre of the heated region. The diameter of the pins is 6.55 mm and they are positioned in order to create a hexagonal lattice with an 8.4 mm pitch. Each pin is held in position by two grids, upstream and downstream the hexagonal duct; inside the FPS, a 1.75 mm diameter wire wrapped around each pin provides

https://doi.org/10.1016/j.nucengdes.2019.110392

instead local support, the axial pitch of the wires being 262 mm. Consequently, 54 sub-channels, (24 interior, 18 edge, 12 corner) can be spotted. Figure 1b also shows the locations housing the detecting instrumentation: 67 thermocouples, represented by the blue sticks, are installed in the FPS at various heights, providing information about temperature on several subchannels and rods.

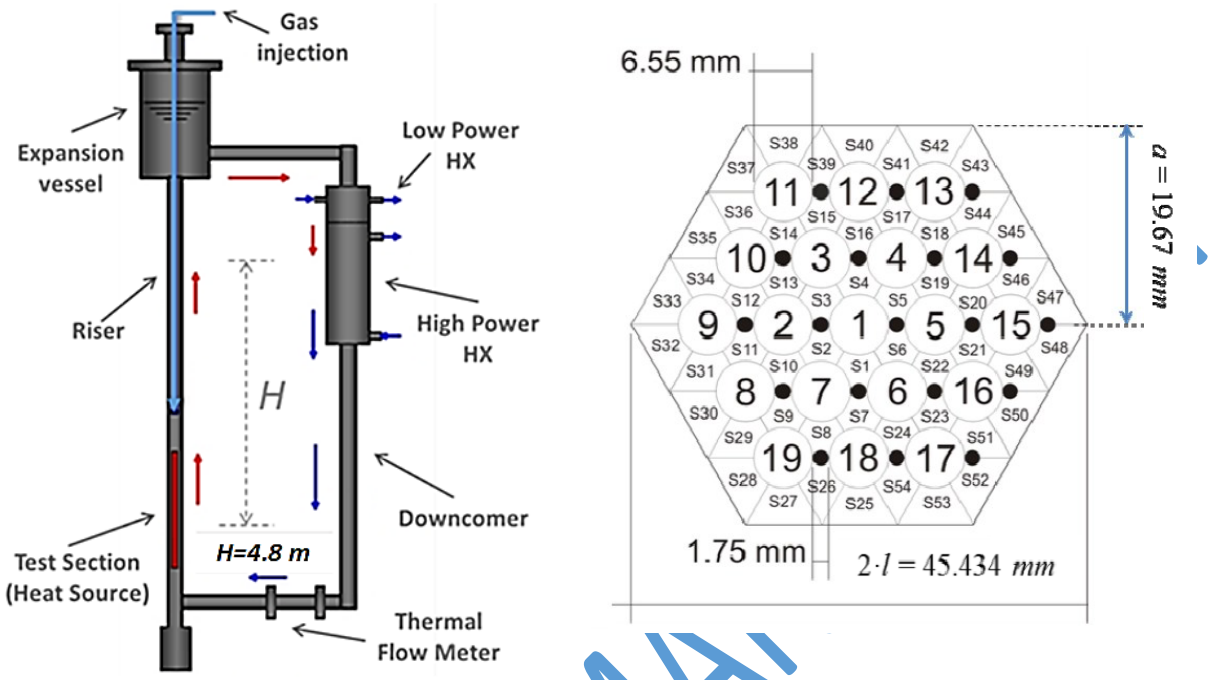

a) *b)*

Figure 1: Schematic layout of the NACIE-UP facility (a) and Sketch of the cross section of the FPS (b) Di Piazza et al., 2016

CFD discretization

The considered domain consists of the FPS test section: a five wire pitches long region was simulated resulting in a computational domain having the total length of 1310 mm. Three main regions may be observed: a first region 617 mm long simulating the unheated entrance region, a 600 mm long region simulating the active region and a final unheated region consisting in the unheated last 93 mm.

In order to comply with the requirements and typical practices adopted when performing CFD calculations, some assumptions were considered when moving from the actual to the simulated geometry. In particular, in order to reduce the computational cost, instead of considering full rods, the pins were simulated as pipes, being convinced that the assumed change does not relevantly impact on the predicted results for steady state simulations. As a consequence, for the heated cases, instead of imposing a volumetric heat source in the central region of the rod, a constant heat flux is imposed on the inner surface of the pins. Another assumption regards the shape of the wrapped wires. In the NACIE-UP facility the wires contribute in maintaining the fuel bundle configuration all along the test section; as a consequence, very narrow passages, in the order of 0.1 mm, exist between the wire and the neighbouring rods. In addition, since a tangency condition is assumed in the test facility between each rod and its wire, even narrower fluid passages can be spotted in the vicinity of the contact

https://doi.org/10.1016/j.nucengdes.2019.110392

point. These occurrences may imply the arise of problems during the meshing process, affecting the capabilities of the meshing tool in reproducing near wall refinements, and stability issues when performing CFD calculations, since they may relevantly impact on the resolution of the continuity, momentum, energy and turbulence equations. As a consequence, a slightly different geometry was assumed in the considered domain; in particular, the wires were immersed for 0.05 mm in the adjacent rod imposing a fillet edge instead of the actual punctual contact.

A further assumption was considered, again, with the aim of reducing the total computational cost of the calculations; in particular, the geometry was scaled down in the axial direction only by a factor of 10 before the meshing operations, it was meshed and then scaled back to the real dimensions. In this way cells elongated in the axial dimension were obtained; however, a refined discretization on transversal planes, allowing the use of low y^+/Low-Re approaches, was maintained yet achieving a lower total cell count. Sensitivity analyses were performed adopting a mesh that is axially more refined, confirming the results obtained with the coarser one, which was consequently considered reliable.

The calculations were performed both adopting Ansys Fluent (2018) and STAR-CCM+ by CD-Adapco (2018): Figure 2 shows an overview of the generated nodalization at the outlet section obtained in the near rod region adopting the meshing tool from Ansys; in Figure 3 a particular of the near rod region, obtained adopting the Ansys (a) and the STAR-CCM+ (b) meshing tool is instead reported.

Table 1 and Table 2 present the mesh size information adopted for both cases: owing to different settings and capabilities of the adopted tools, slightly different values were adopted for the two generated meshes. The imposed settings allow obtaining a wall y^+ value lower than unity for most of the investigated operating conditions; only for cases involving a very high mass flux this threshold value is slightly exceeded. As a consequence, a sufficient number of cells lies in the viscous sub-layer and transition layer region, providing a suitable discretization of the near wall behaviour, which is required by the adopted turbulence models and selected wall approaches. In particular, the low y^+/ Low-Re approach was adopted for all the performed calculations; a model from the k-ε and k-ω family was selected from both the commercial CFD codes. The selected turbulence models were the SST k-ω (Menter, 1994) for both Ansys Fluent and STAR-CCM+, the Standard k-ε with enhanced wall treatment and the Lien k-ε (Lien et al., 1996) model in Ansys Fluent and STAR-CCM+ respectively.

https://doi.org/10.1016/j.nucengdes.2019.110392

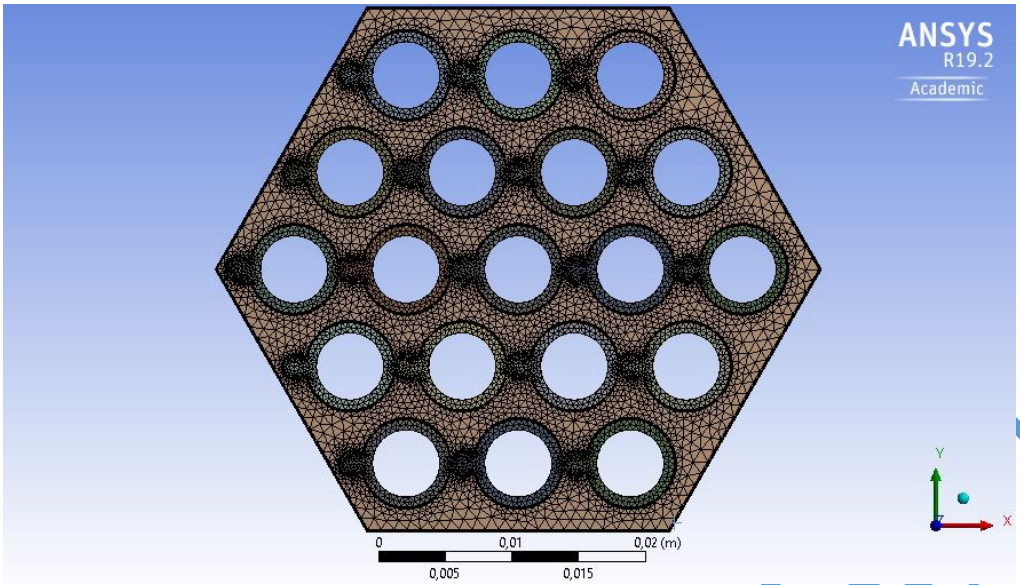

Figure 2: Mesh generated adopting the Ansys meshing tool: outlet section overview

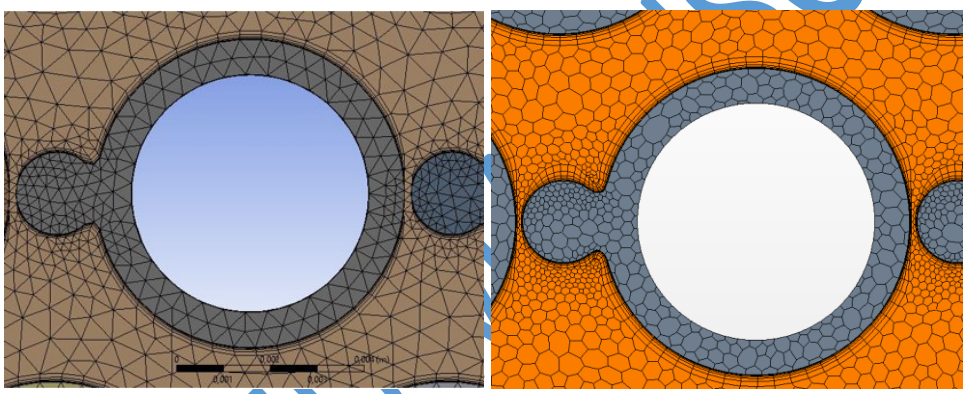

a) *b)*

Figure 3: Particular of the near rod region, mesh generated by the Ansys meshing tool (a) and the STAR-CCM+ meshing tool (b)

Table 1: Fluent Mesh settings

Fluid Domain	
Base size [mm]	1
Local Minimum size [mm]	0.2
Curvature Normal Angle [°]	8
First Layer Thickness	0.01
Maximum Layers	5
Growth Rate	1.7
Solid Domain	
Base size [mm]	1
Local Minimum size [mm]	0.5
Curvature Normal Angle [°]	8
Total N° of cells	24668290

https://doi.org/10.1016/j.nucengdes.2019.110392

Table 2: STAR-CCM+ meshing tool settings

Fluid Domain	
Base size [mm]	0.5
Surface Curvature [points/circle]	50
Max points/circle	200
Prism layer thickness [mm]	0.25
Number of prism layers	6
Prism layer stretching	1.7
Solid Domain	
Base size [mm]	0.5
Surface Curvature [points/circle]	60
Max points/circle	200
Total N° of cells	20675590

OBTAINED RESULTS

Pressure Drops and Friction Factor predictions

As anticipated in the previous section, one of the objectives of the present work was assessing the capabilities of the selected codes in predicting the pressure drops, and consequently the friction factor, comparing the obtained results with the ones provided by correlations available in the literature.

In particular, the correlation by Cheng and Todreas (1986) was selected as a reference as it showed interesting capabilities in the frame of other experiences, involving e.g. the RELAP5 system code. Finding a correlation that fits sufficiently well the experimental and calculated data is of primary importance as it may provide relevant information in view of possible coupled calculations adopting both CFD and STH codes. This is in particular relevant for facilitating and speeding up the synchronization process between the adopted CFD and STH codes required at the beginning of each coupled calculation for the sake of setting the system initial conditions.

Since the detailed Cheng and Todreas (1986) correlation requires defining a consistent number of steps, parameters and coefficients for a clear and complete description, the reader is remanded to Chen et al. (2014) for further information. The results of the application of the correlation will consequently be reported in the next figures without any further detail.

Concerning the calculation of the friction factor coefficient from CFD results, it must be remarked that it was obtained starting from the calculated friction pressure drop between the beginning and the end of the active length, being a region far enough in terms of hydraulic diameters from the boundaries, thus avoiding possible entrance and discharge effects. The friction factor (f) was subsequently estimated adopting the relation hereinafter reported.

https://doi.org/10.1016/j.nucengdes.2019.110392

$$f = \frac{2\,\Delta P_{fric}}{\rho\, v_{mean}^2}\frac{D_{eq}}{L} \quad (1)$$

The adopted v_{mean} value is calculated performing an area-weighted average on some selected transversal sections from the CFD calculation. The equivalent diameter D_{eq} was instead calculated through the relation below which is broadly adopted in literature, in which A represents the flow section and P_w the wetted perimeter.

$$D_{eq} = \frac{4\,A}{P_w} \quad (2)$$

It is remarked here that the adopted D_{eq} is the one which is coherent with the modified geometry considered in the performed CFD calculations, which assumes the immersed wire. This value is about 10% larger than the one calculated analytically considering the real wrap geometry; nevertheless, assuming the one or the other value does not relevantly affect the quality of the prediction or changes the conclusion that can be drawn, since the predicted friction factor would remain inside the uncertainty range of the correlation.

Figure 4 reports the average friction factor calculated from CFD results and the one provided by some selected correlations as a function of Reynolds number, for an imposed LBE temperature of 250°C. As it can be observed, the CFD results reproduces quite well the trend provided by the Cheng and Todreas (1986) correlation, whose uncertainty range is reported as well (dashed lines). In literature, the Rehme (1973) correlation is also considered as best-fit correlation (see e.g. Kennedy et al., 2015), nevertheless, according to the present CFD comparison, it seems underestimating the friction factor prediction in the laminar flow region. The Chen et al. (2018) correlation, which updates the one developed by Cheng and Todreas (1986) is reported as well: all the CFD predictions lay well inside its uncertainty range (not shown here).

As a general comment on these results, it can be stated that all the considered turbulence models seem able to reproduce the transition between laminar and turbulence conditions in accordance with the Cheng and Todreas correlation: this may be relevant for calculations involving transient conditions with mass flows ranging from laminar to almost fully developed turbulent conditions, as the ones that may be faced in the NACIE-UP facility.

Figure 5 reports instead a sensitivity analysis concerning the effect of fluid properties variation; in particular an imposed temperature value of 350°C is considered here. As it can be observed, no relevant changes are highlighted in comparison to the previous Figure 4, thus suggesting that the adopted models seem able to reproduce the obtained trend independently of the adopted fluid properties.

Among the considered turbulence models, the SST k-ω model reports the best performance both in the ANSYS Fluent and STAR-CCM+ applications, it was consequently chosen for the post-test analyses reported in the next sections.

https://doi.org/10.1016/j.nucengdes.2019.110392

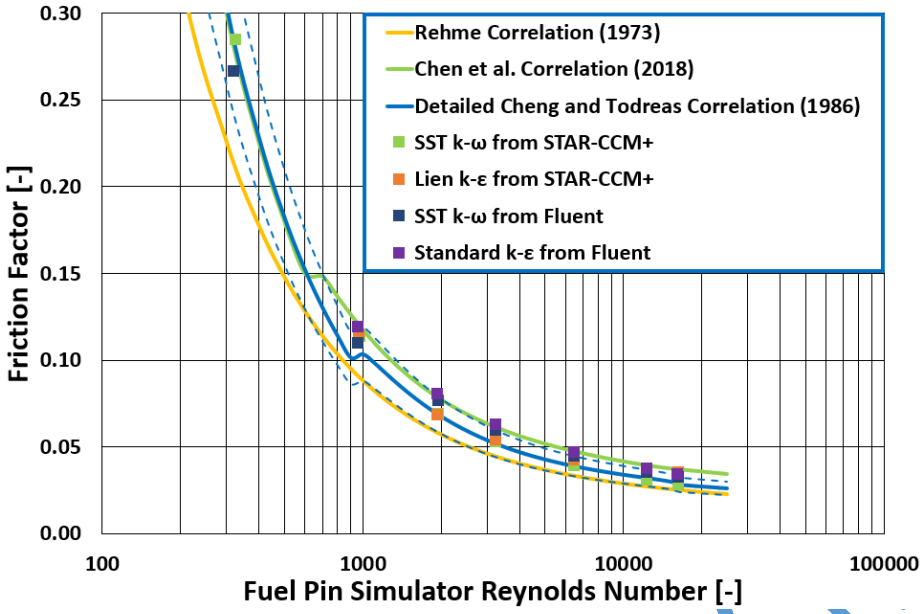

Figure 4: Comparison of the calculated Friction Factor coefficient obtained by CFD codes and the one provided by some selected correlations for an imposed temperature of 250°C

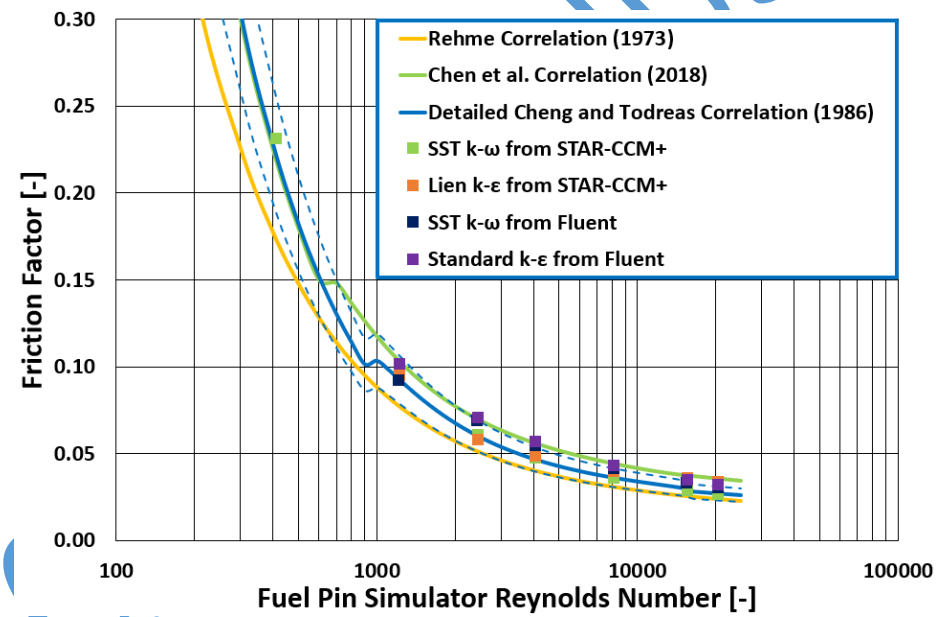

Figure 5: Comparison of the calculated Friction Factor coefficient obtained by CFD codes and the one provided by provided by some selected correlations for an imposed temperature of 350°C

Post-test calculations

Data processing and simplifying hypotheses

In the present section some of the available experimental results are compared with the CFD predictions obtained adopting the above mentioned nodalization and turbulence models; the calculations were preliminarily performed adopting only Ansys Fluent code.

https://doi.org/10.1016/j.nucengdes.2019.110392

During the NACIE-UP H2020-SESAME (Di Piazza et al., 2017), three transient conditions involving both power and argon mass flow rate transition were considered in order to investigate the natural circulation phenomena occurring in the experimental facility. Before the beginning of each transient, steady state conditions were reached, the test ended when new steady state conditions were achieved again. In the present paper, three steady state conditions were considered, being convinced they are representative enough of the investigated operating conditions. In particular, conditions involving the maximum provided power (100 kW) and different Argon mass flow rates were considered. For sake of clarity, it is here again highlighted that the imposed Argon mass flow rate, inserted downstream the FPS, strongly influences the obtained mass flow rate, implying mixed circulation conditions. Table 3 presents the nominal operating conditions investigated in the present work. The uncertainties related to the various quantities are ±1°C for temperature, ±5% and ±5.5% for LBE and gas mass flow rate respectively and ±2% for the supplied power.

Table 3: Considered Nominal Operating Conditions

Case	T_{in} [°C]	$\dot{m}_{lbe}$ [kg/s]	$\dot{m}_{Ar}$ [Nl/min]	Q [kW]
Test-1 – Pre-Transient steady state	250.8	3.81	20	50
Test-1 – Post-Transient steady state	245.7	3.09	10	50
Test-3 – Pre-Transient steady state	280	4.32	20	100

The values reported in *Table 3* represent a time-average of the experimental data. An energy balance analysis is hence performed for every case, trying to understand if the measured supplied power is compatible with the amount of energy received by the fluid.

In addition, in similarity with the work by Di Piazza et al., (2016) and Angelucci et al., (2018), an attempt is made for investigating the possible presence of anomalous power distribution along the test section. Figure 6 reports the location of embedded and bulk thermocouples for each of the three selected transversal planes A, B and C.

https://doi.org/10.1016/j.nucengdes.2019.110392

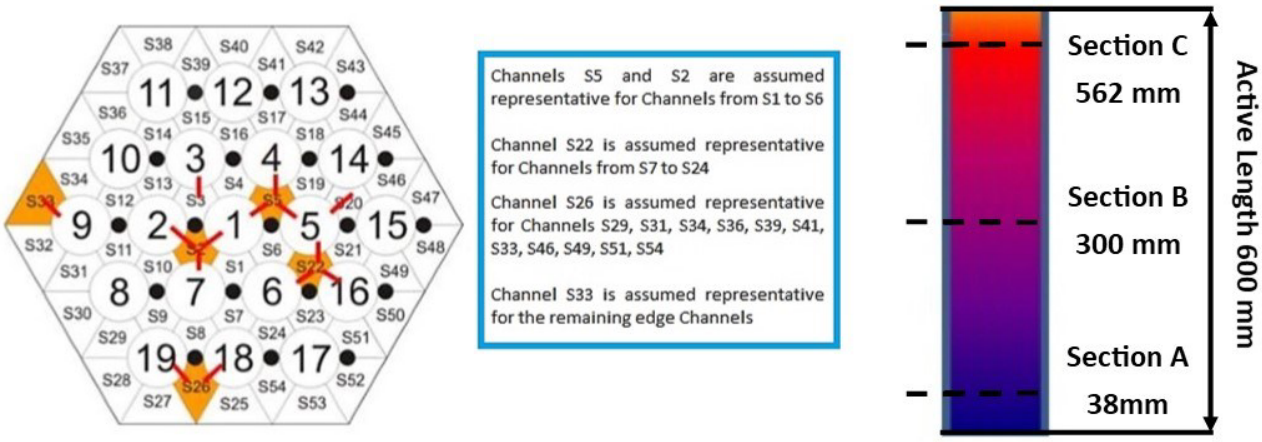

Figure 6: Cross-sectional locations of the thermocouples and subchannel information

The temperatures measured by the thermocouples positioned in the bulk of channels S2, S5, S22, S26 and S33 are used for the sake of calculating an approximated bulk temperature for each section. In particular, considering that the measured channels may be assumed as representative of other channels facing similar boundary conditions, some area based weighting factor, reported below, were used in Eq. (4), providing an estimation of the local bulk temperature. The adopted weighting factor w_k were calculated taking into account the average obstruction due to both pins and wires, the mass flow rates flowing in each sub-channel were considered as well in the weighting process; they are:

$$w_2 \approx 0.0573\,;\ w_5 \approx 0.0573\,;\ w_{22} \approx 0.3437\,;\ w_{26} \approx 0.2059\,;\ w_{33} \approx 0.3358 \quad (3)$$

$$T_{b,section} \approx T_{S2} \cdot w_2 + T_{S5} \cdot w_5 + T_{S22} \cdot w_{22} + T_{S26} \cdot w_{26} + T_{S33} \cdot w_{33} \quad (4)$$

TC-09, the thermocouple positioned in sub-channel S26 at Section B, supplied unreliable measurements and for this reason was not considered in the post-processing, thus an estimation of the bulk temperature for Section B cannot be performed. Bulk temperature value was consequently calculated only for Sections A and C; the two values were then adopted for the sake of estimating the inlet and outlet temperature of the heated test section, assuming a linear bulk temperature trend along the hexagonal duct. Figure 7 shows the described process for Test-1 in Post-Transient conditions; Table 4 presents instead the estimated inlet and outlet LBE temperature values, to be compared with the average values provided by TC101 and TC102, positioned well before and after the theoretical heated section.

https://doi.org/10.1016/j.nucengdes.2019.110392

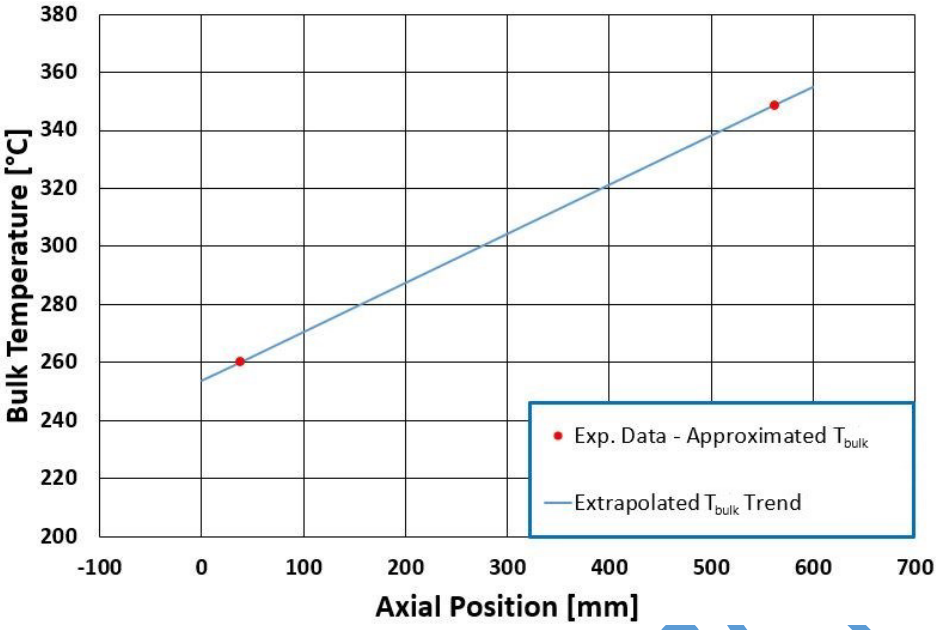

Figure 7: Approximated and extrapolated LBE bulk temperature values for Test-1, Post-transient conditions

Table 4: Measured and extrapolated LBE temperature values at the inlet and outlet sections of FPS. Measured temperatures uncertainty ±1

Case	T101 [°C]	T_{in} (extrapolated) [°C]	T102 [°C]	T_{out} (extrapolated) [°C]
Test-1 – Pre-Transient steady state	250.95	257.22	339.81	340.38
Test-1 – Post-Transient steady state	245.72	253.73	354.69	354.88
Test-3 – Pre-Transient steady state	281.54	294.63	440.07	442.74

As it can be observed in Table 4, the measured and estimated inlet temperature values seem not to be sufficiently close; for the outlet section values instead, considering that the uncertainties may even be of the order of 1°C, we may assume that compatible enough values were obtained.

Consequently, considering the assumed estimating process reliable, we may speculate that the supplied power is not provided in the theorical heated section only, but is instead partly supplied in the upstream section after the T101 measurement point, in the range of 6-10% of the nominal power. Calculations trying to take into account this possible scenario were performed while potential power dissipations towards the environment were neglected, since the global energy balance, taking into account the measurements uncertainties, is respected.

https://doi.org/10.1016/j.nucengdes.2019.110392

The obtained results are reported and commented in the next subsections; the imposed inlet and mass flow conditions are the nominal ones, which are reported in Table 3, the SST k-ω turbulence model was adopted for all the calculations.

SESAME Test-1 – Pre-Transient steady state

Figure 8 reports the comparison between the experimental data and CFD predictions for some selected thermocouples locations. A sensitivity analysis concerning the adopted turbulent Prandtl number (Pr_t) is also performed. In the available literature (see e.g. Cheng and Tak, 2006) a Pr_t value in the range 1-1.5 is required for liquid metals. It can be observed that the predictions taking into account different turbulent Prandtl number values do not show relevant changes, thus suggesting that, at least in this case, it only implies a limited impact on the obtained results.

It is interesting also observing the trend obtained considering an imposed power source not only in the heated section but also in the upstream region, a hypothesis suggested by the analysis of the bulk enthalpy trend proposed in the previous section. The extrapolated bulk temperature trends, together with energy balance, suggests that 91.7% of the nominal power was imposed in the heated section, while the remaining part was supplied in the upstream unheated section. Nevertheless, Figure 8 shows that imposing these particular boundary conditions provides results very close to the ones obtained with the hypothesis of uniform heat flux supplied in the heated section only.

Figure 9 reports instead the values measured on Pin 3 together with channel bulk temperature measurements trends, in a plot reporting the axial position on the abscissa; the considered CFD prediction is the one assuming $Pr_t = 1.5$ and a uniform heat source in the heated section only. It can be observed that, while for axial positions lower than 300 mm a very good prediction is obtained, some overestimations are instead reported for the second part of the heated section. These discrepancies, together with the obvious limits of a CFD prediction, may be due to possible non-homogeneity in the supplied power or mispositioning of the thermocouples. An example of the uncertainties that may be faced when considering the experimental data, is the comparison between the measured data in Channel 2 and Channel 5, which, ideally, should provide similar values (see Figure 6). As it can be noted in Figure 9, in particular for the first and last reading, the measured temperature in Channel 2 is higher than the one measured in Channel 5 reporting differences also of the order of 10°C. Considering Channel 5, the CFD prediction is very close to the measured value for the 562 mm section; this suggests that the obtained results may be considered sufficiently reliable and promising in view of future analyses.

SESAME Test-1 – Post-Transient steady state

The comparison of CFD and experimental data is reported in Figure 10 taking into account different Pr_t values and heat flux distributions: as occurred for the previously considered Pre-Transient conditions, the CFD calculation manages to reproduce quite well the measured values. One more time, comparing the values in the first and final part of the heated section (see also Figure 11), an overestimation of the measured values can be

https://doi.org/10.1016/j.nucengdes.2019.110392

observed for axial positions downstream 300 mm, while compatible values are instead predicted upstream. Again, though discrepancies between measured and calculated values may seem significant, in particular for the final part of the heated section, after taking into account the possible uncertainties the results can be considered sufficiently reliable and representative of the general trend.

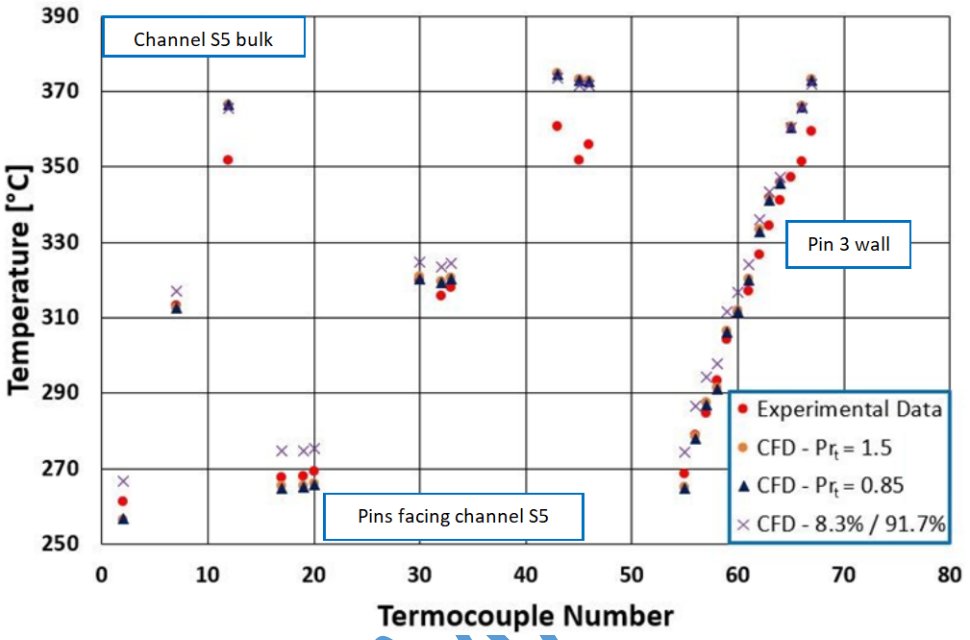

Figure 8: Test-1, Pre-Transient conditions: comparison of experimental data and CFD calculations

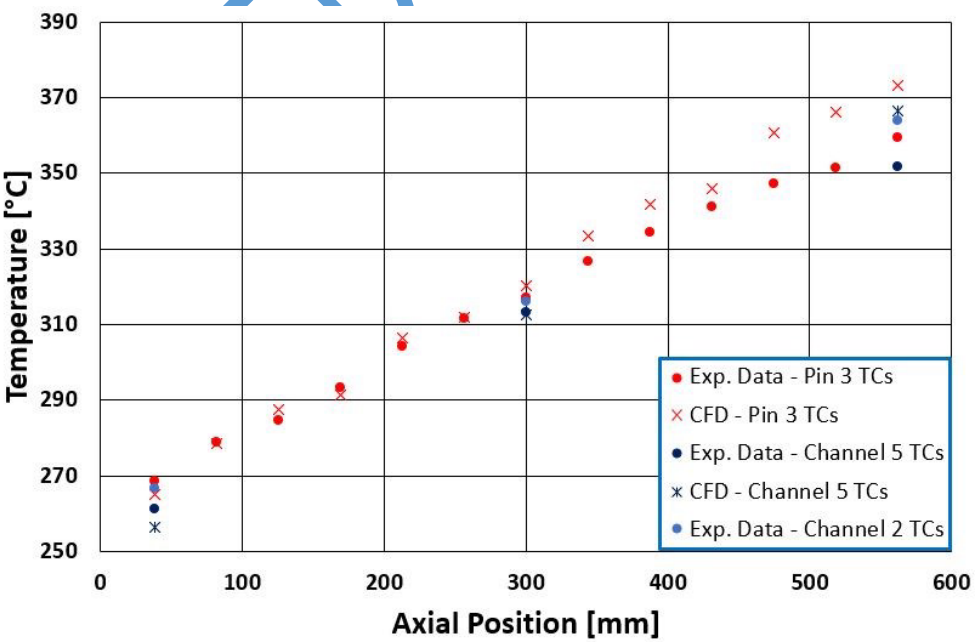

Figure 9: Test-1, Pre-Transient conditions: comparison of experimental data and CFD calculations, particular of Pin 3 surface

https://doi.org/10.1016/j.nucengdes.2019.110392

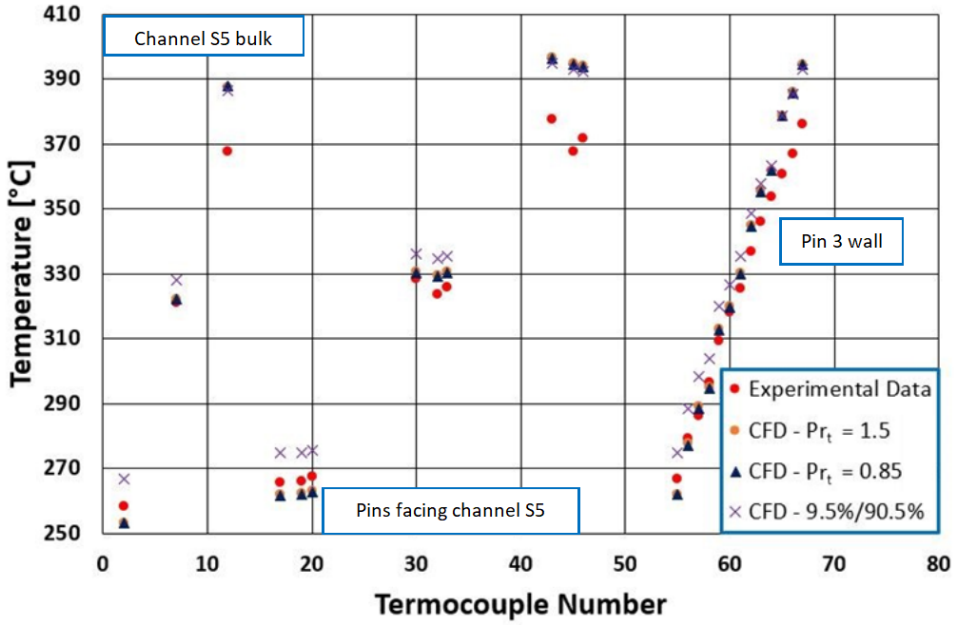

Figure 10: Test-1, Post-Transient conditions: comparison of experimental data and CFD calculations

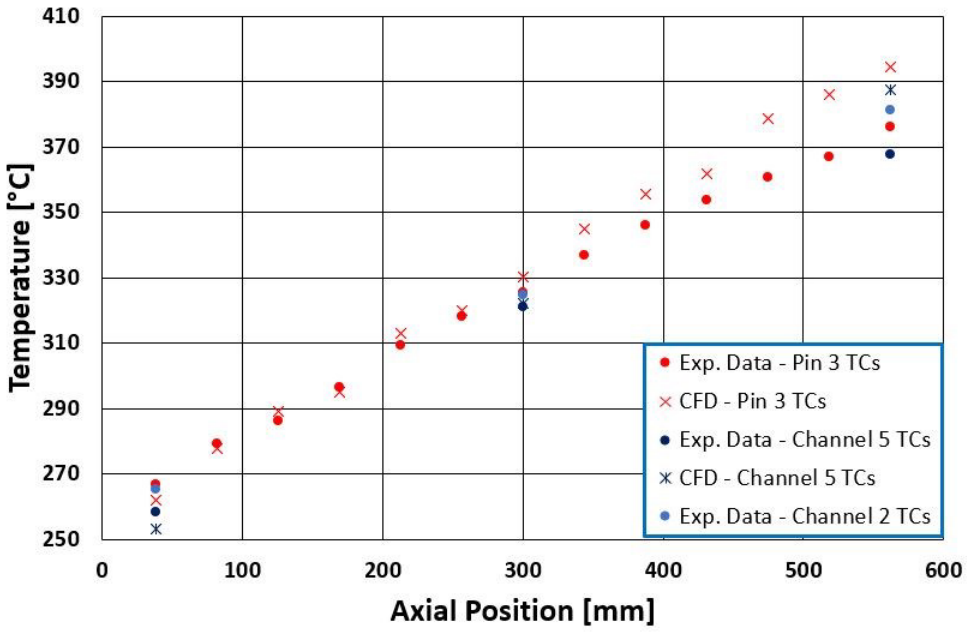

Figure 11: Test-1, Post-Transient conditions: comparison of experimental data and CFD calculations, particular of Pin 3 surface

SESAME Test-3 – Pre-Transient steady state

Figure 12 shows the comparison of the measured and calculated trends for the Pre-Transient conditions for Test-3; again different heat flux distributions and Pr_t values were considered. The predictions are once again sufficiently close to the experimental data and no relevant changes can be observed both when changing the turbulent Prandtl number or the power distribution.

https://doi.org/10.1016/j.nucengdes.2019.110392

As happened in the previous cases, even here an overestimation of the measured trends can be observed in the final part of the test section (Figure 13); the uncertainties in the positioning of the thermocouples, together with possible non-uniformities in the power distribution may lead to the observed discrepancies.

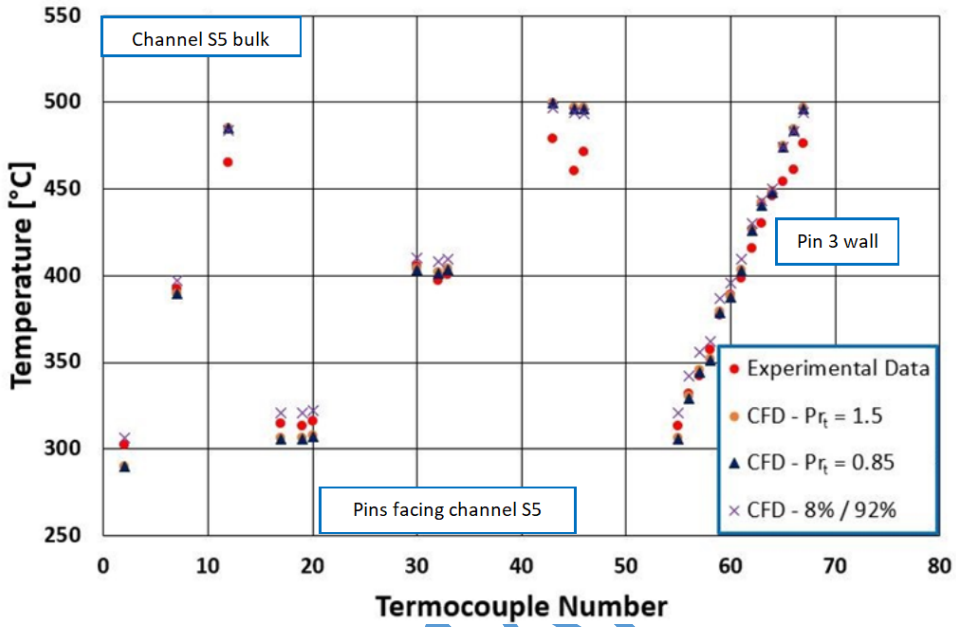

Figure 12: Test-3, Pre-Transient conditions: comparison of experimental data and CFD calculations

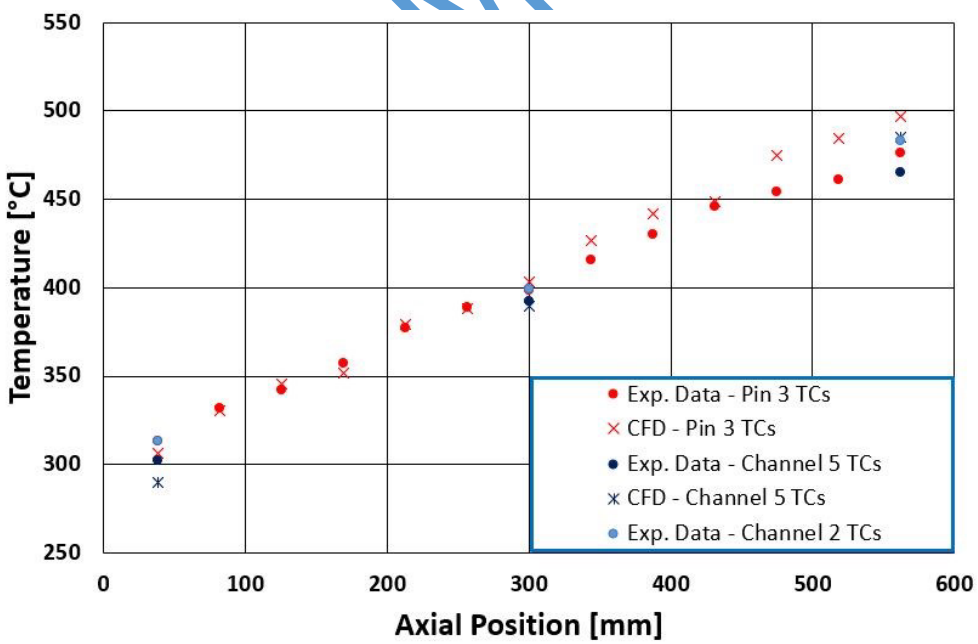

Figure 13: Test-3, Pre-Transient conditions: comparison of experimental data and CFD calculations, particular of Pin 3 surface

https://doi.org/10.1016/j.nucengdes.2019.110392

CONCLUSIONS

The present paper describes the numerical analysis performed in support of the NACIE-UP experimental campaign both providing information about the fluid-dynamic and thermodynamic involved phenomena.

In particular, the analysis of the pressure drops showed an interesting matching between the CFD calculations and the predictions provided by the Cheng and Todreas (1986) correlation, which was purposely developed for predicting wire-wrapped hexagonal array pin bundles. Both Ansys Fluent and STAR-CCM+ CFD codes provided good estimations of the pressure drops, reporting better matching with the selected correlation when adopting the SST k-ω turbulence model, which was consequently used for post-test calculations. This matching suggests promising capabilities in view of applications involving Fluent/RELAP5 coupled calculations; it is in fact expected that a more coherent estimation of the pressure drops by the two codes could really improve the quality of the obtained results.

Post-test analyses were performed as well. The obtained results show good capabilities in predicting the steady state conditions observed during the experimental campaign, suggesting that the technique adopted for the discretization of the domain was sufficiently reliable. Temperature predictions reproduced sufficiently well the experimental results, reporting temperature overestimations in the final part of the heated section. Sensitivity analyses were performed in order to understand the influence of the imposed parameters; different boundary conditions were considered showing only a limited impact on the obtained results. Changes in the imposed turbulent Prandtl number were considered as well and no relevant changes in the predicted temperature trends were observed.

ACKNOWLEDGEMENT

This work was performed in the framework of the H2020 SESAME project. This project has received funding from the Euratom research and training program 2014.2018 under grant agreement No 654935.

https://doi.org/10.1016/j.nucengdes.2019.110392

REFERENCES

ANSYS, Inc., "*ANSYS Fluent User's Guide, Release 19.2"*, August 2018.

Angelucci, M., Di Piazza, I., Martelli, D., "Experimental campaign on the HLM loop NACIE-UP with instrumented wire-spaced fuel pin simulator", Nucl. Eng. Des., vil 332, pp. 137-146, 2018

CD-Adapco, "*USER GUIDE STAR-CCM+ Version 13.06.011",* 2018.

Chen S. K., Todreas N. E. , Nguyen N. T., *"Evaluation of existing correlations for the prediction of pressure drop in wire-wrapped hexagonal array pin bundles"*, Nucl. Eng. Des., vol. 267, no. December 2013, pp. 109–131, 2014.

Chen S. K., Chen, Y. M., Todreas N. E., *"The upgraded Cheng and Todreas correlation for pressure drop in hexagonal wire-wrapped rod bundles"*, Nucl. Eng. Des., vol. 335 (pp. 356–373, 2018.

Cheng X., Tak N.I., "*CFD analysis of thermal-hydraulic behavior of heavy liquid metals in sub channels*, Nucl. Eng. Des. 236, pp.1874-1885, 2006.

Cheng, S.K., Todreas, N.E., "*Hydrodynamic models and correlations for bare and wire-wrapped hexagonal rod bundles – bundle friction factors, sub-channel friction factor and mixing parameters"*. Nuclear Engineering and Design 92, 227-251, 1986.

Di Piazza et al., "Nacie-UP: an heavy liquid metal loop for mixed convection experiments with instrumented pin bundle" HLMC-2013, 2013.

Di Piazza, I., Angelucci, M., Marinari, R., Tarantino, M., Forgione, N., "*Heat transfer on HLM cooled wire-spaced fuel pin bundle simulator in the NACIE-UP facility"*. Nuclear Engineering and Design 300, 256-267, 2016.

Di Piazza, I., Angelucci, M., Polazzi, G., Sermenghi, V., "D4.9 – NACIE-UP set-up for PLOFA", Deliverable SESAME Workflow - D4.9 - Issued on 2016-01-13.

Di Piazza, I., Angelucci, M., Polazzi, G., Sermenghi, V., "D4.10 – NACIE-UP data for PLOFA experiment", Deliverable SESAME – 654935 – D4.10 - version 0 issued on 01/09/2017.

Forgione, N., Barone, G., Martelli, D., Ambrosini, W., Lo Frano, R., Pucciarelli, A., "*NACIE_UP RELAP5/FLUENT simulations",* Deliverable D5.21 for WP5, Task 5.4 of SESAME project, 2019.

Generation IV International Forum (GIF). "*Technology Roadmap Update for Generation IV Nuclear Energy Systems*", 2014.

Gonfiotti, B., Barone, G., Angelucci, M., Martelli, D., Forgione, N., Del Nevo, A., Tarantino, M., "*Thernal hydraulic analys of the circe-hero pool-type facility*", International Conference on Nuclear Engineering, Proceedings, ICONE Volume 6B, 20182018 26th International Conference

https://doi.org/10.1016/j.nucengdes.2019.110392

on Nuclear Engineering, ICONE 2018; London; United Kingdom; 22 July 2018 through 26 July 2018; Code 141167

Kennedy, G., Van Tichelen, K., Doolaard, H., *"Experimental investigation of the pressure loss characteristics of the full-scale MYRRHA fuel bundle in the COMPLOT LBE facility"*. NURETH-16, Chicago, IL, August 30-September 4, 2015.

Lien, F.S., Chen, W.L., Leschziner, M.A., *"Low-Reynolds number eddy viscosity modelling based on non-linear stress-strain/vorticity relations"*. Proceedings of the 3rd Symposium on Engineering Turbulence Modelling and Measurements, 27-29 May, 1996, Crete, Greece.

Marinari R., *"Pre-test CFD analysis of the rod bundle experiment in the Heavy Liquid Metal facility NACIE-UP"*, Master of Science Thesis, University of Pisa, 2014.

Marinari R., Di Piazza, I., Angelucci, M., Martelli, D., "*Post-Test CFD analysis of non-uniformly heated 19-pin fuel bundle cooled by HLM*". Proceedings of the 2018 26th International Conference on Nuclear Engineering ICONE 26, July 22-26, 2018, London, England

Martelli, D., Forgione, N., Barone, G., Del Nevo, A., Di Piazza, I., Tarantino, M., "*Coupled simulations of natural and forced circulation tests in NACIE facility using relap5 and Ansys fluent codes"* 2014 22nd International Conference on Nuclear Engineering, ICONE 2014; Prague; Czech Republic; 7 July 2014 through 11 July 2014; Code 109131.

Martelli, D., Marinari, R., Barone, G., Di Piazza, I., Tarantino, M., "*CFD thermo-hydraulic analysis of the CIRCE fuel bundle"*, Annals of Nuclear Energy, Volume 103, 1 May 2017, Pages 294-305, 2017a

Martelli, D., Forgione, N., Barone, G., Di Piazza, I., "Coupled simulations of the NACIE facility using RELAP5 and ANSYS FLUENT codes", Annals of Nuclear Energy, Vol. 101, pp. 408-418, 2017b.

Narcisi, V., Giannetti, F., Tarantino, M., Martelli, D., Caruso, G., *"Pool temperature stratification analysis of CIRCE-ICE facility with RELAP5-3D© model and comparison with experimental tests"*, Journal of Physics: Conference Series, Volume 923, Issue 1, 20 November 2017, Article number 01200635th Italian Union of Thermo-Fluid Dynamics Heat Transfer Conference, UIT 2017; Faculty of Engineering, Marche Polytechnic University Ancona; Italy; 26 June 2017 through 28 June 2017; Code 131974

Menter, F.R., "*Two-equation eddy-viscosity turbulence modelling for engineering applications*". AIAA Journal 32(8) pp. 1598-1605, 1994.

https://doi.org/10.1016/j.nucengdes.2019.110392

Pesetti, A., Forgione, N., Narcisi, V., Lorusso, P., Giannetti, F., Tarantino, M., "ENEA CIRCE-HERO test facility: geometry and instrumentation description", ENEA report for Project H2020 SESAME Project WP5.2, Ref. CI-I-R-343, 2018.

Tarantino, M., Agostini, P., Benamati, G., Coccoluto, G., Gaggini, P., Labanti, V., Venturi, G., Class, A., Liftin, K., Forgione, N., Moreau, V., "*Integral Circulation Experiment: Thermal-hydraulic simulator of a heavy liquid metal reactor*", Journal of Nuclear Materials 415r, 433-448, 2011